Computers and Chemical Engineering 178 (2023) 108387

Contents lists available at ScienceDirect

Computers and Chemical Engineering

journal homepage: www.elsevier.com/locate/compchemeng

Enhanced single-loop control of a moving bed temperature swing adsorption CO_2 capture process

Vidar T. Skjervold *, Lars O. Nord

Department of Energy and Process Engineering, NTNU - Norwegian University of Science and Technology, Trondheim, Norway

ARTICLE INFO

Keywords:
MBTSA
Post-combustion CO_2 capture
Process modeling
Process control
Adaptive tuning
Dynamic simulations

ABSTRACT

Using a model in gPROMS, we study a Zeolite 13X-based moving bed temperature swing adsorption (MBTSA) process designed to capture CO_2 from a coal-fired power plant. Two enhanced single-loop control strategies were compared to a proportional-integral configuration for variations in power plant load, control variable setpoints, flue gas CO_2 concentration and external heat source temperature. Measurement delays were also investigated. Adaptive adjustment of controller parameters with system load gave smoother and narrower manipulated variable profiles and efficient CO_2 recovery setpoint tracking. The controller gain is the most important parameter for adaptive tuning. A combined feedback and feedforward scheme showed improved control of the regenerated sorbent temperature, possibly due to better decoupling of the higher-level control loops. When delays were considered, the investigated strategies significantly outperformed the reference case for CO_2 recovery control. The results demonstrate that the MBTSA process can be efficiently controlled for several disturbances and changes in operation.

1. Introduction

1.1. Background and motivation

In 2022, global energy-related CO_2 emissions reached a previously unprecedented level of 36.8 Gt, an increase of 0.9% compared to 2021 (IEA, 2023). To mitigate the effects of global warming and reach the goals of the Paris Agreement, these emissions must be significantly reduced in the coming years. The European Union aims at an economy with net zero greenhouse gas emissions by 2050, as outlined in the European Green Deal (European Commission, 2019). Fossil fuel-based power plants stand for almost two thirds of electricity generation, leading to approximately 40% of global energy-related emissions (IEA, 2020). In the transition to an energy system based on renewable energy sources, it is likely that CO_2 capture from thermal power plants will be necessary to reduce emissions while ensuring security of energy supply. The Intergovernmental Panel on Climate Change estimates wide deployment of carbon capture and storage on both natural gas and coal-fired power plants in pathways limiting the global temperature increase to 1.5 °C above pre-industrial levels (IPCC, 2018).

Post-combustion CO_2 capture is suitable for existing power plants, since it can be retrofitted without requiring major changes to the combustion process (Kazemifar, 2022). The state-of-the-art technology for post-combustion CO_2 capture is chemical absorption, which has been proven at commercial scale. However, other technologies such as membrane separation, cryogenic distillation, adsorption and hybrid processes have reached high technology readiness levels and could be viable alternatives (Dziejarski et al., 2023). Adsorption-based processes are considered promising because they have the potential for reduced energy requirements compared to standard amine-based absorption (Raganati et al., 2021). These processes can vary greatly, depending on the choice of reactor configuration, regeneration mode and adsorbent material. In this work, a moving bed temperature swing adsorption (MBTSA) process with a Zeolite 13X adsorbent is considered. The primary advantage of moving beds compared to the fixed bed configuration is the possibility of continuous operation, which avoids the complex operation cycles associated with switching between operation modes (Dhoke et al., 2021). Temperature swings are suitable for CO_2 capture from power plants due to the potential availability of low-grade thermal energy for desorption and the significant electrical power requirements associated with vacuum or pressure swings of the near-atmospheric flue gas discharged from the power plant (Zhao et al., 2019). Zeolite-based adsorbents have fast adsorption kinetics and low regeneration duties, making them attractive for post-combustion CO_2 capture (Samanta et al., 2012). Potential drawbacks of zeolites are their

* Corresponding author.
E-mail address: vidar.t.skjervold@ntnu.no (V.T. Skjervold).

https://doi.org/10.1016/j.compchemeng.2023.108387
Received 15 May 2023; Received in revised form 5 July 2023; Accepted 7 August 2023
Available online 9 August 2023

Nomenclature

Acronyms

CV	controlled variable
FF	feedforward
IAE	integral absolute error
MBTSA	moving bed temperature-swing adsorption
MEA	monoethanolamine
MPC	model predictive control
MV	manipulated variable
PI	proportional-integral
PID	proportional-integral-derivative
RGA	relative gain array
SIMC	simplified internal model control
SRD	specific regeneration duty

Latin symbols

$a^{'}$	particle specific area, $m^2\ m^{-3}$
A_i	first single-component Virial coefficient, kg mol^{-1}
A_{ij}	first multi-component Virial coefficient, kg mol^{-1}
B	controller bias
B_i	second single-component Virial coefficients of component i, $kg^2\ mol^{-2}$
B_{ijk}	second multi-component Virial coefficient, $kg^2\ mol^{-2}$
Bi_i	biot number of component i
c	controller transfer function
$c_{p,f}$	specific heat of the heating/cooling fluid, J $kg^{-1}K^{-1}$
$c_{p,pk}$	specific heat of the packing material, J $kg^{-1}K^{-1}$
$c_{p,s}$	specific heat of the adsorbent, J $kg^{-1}K^{-1}$
$c_{p,w}$	specific heat of the heat exchanger tubes wall, J $kg^{-1}K^{-1}$
$\widehat{c}_p$	molar heat of gas mixture at constant pressure, J $mol^{-1}\ K^{-1}$
$\widehat{c}_v$	molar heat of gas mixture at constant volume, J $mol^{-1}\ K^{-1}$
C_i	concentration of component i in bulk gas phase, mol m^{-3}
$C_{p,i}$	concentration of component i in the macropores, mol m^{-3}
C_T	total molar gas concentration in bulk phase, mol m^{-3}
d	disturbance
d_p	particle diameter, m
$D_{c,i}$	micropores/crystals diffusivity of component i, $m^2\ s^{-1}$
$D_{p,i}$	macropore diffusivity of component i, $m^2\ s^{-1}$
$D_{z,i}$	axial dispersion coefficient of component i, $m^2\ s^{-1}$
e	controller error, -
g	transfer function
I	controller integral term
k	process gain
K_c	controller gain
$k_{f,i}$	film mass transfer coefficient of component i, m s^{-1}
K_i	equilibrium constant of component i, mol kg^{-1} kPa^{-1}
K^{∞}	equilibrium constant at infinite temperature, mol kg^{-1} kPa^{-1}
L_x	tubes length along the flow direction, m
L_z	tubes length along vertical axis, m
$\dot{m}$	mass flow rate, kg s^{-1}
h_{gs}	heat transfer coefficient between the gas and the solid, J $s^{-1}m^{-2}\ K^{-1}$
h_{fw}	heat transfer coefficient between the fluid and the tubes wall, J $s^{-1}\ m^{-2}\ K^{-1}$
h_{gw}	heat transfer coefficient between the gas and the tubes wall, J $s^{-1}m^{-2}\ K^{-1}$
P	total pressure of the gas mixture, Pa
P	controller proportional term
P_i	partial pressure of component i, bar
q_i	adsorbed phase concentration of component i, mol kg^{-1}
q_i^*	adsorbed concentration of component i at equilibrium, mol kg^{-1}
R	ideal gas constant, J $K^{-1}mol^{-1}$
r_c	crystals/micropore radius, m
r_p	particle radius, m
s	Laplace variable, s^{-1}
t	time, s
T	temperature of the gas phase, K
T_f	temperature of the heating/cooling fluid, K
T_s	temperature of the solid phase, K
T_w	temperature of the heat exchanger tubes wall, K
u	superficial gas velocity, m s^{-1}
u	manipulated variable
$u^{'}$	ratio calculated by outer feedback loop
v_s	velocity of the solid phase, m s^{-1}
y	controlled variable
y_{SP}	controlled variable setpoint
Y_i	molar fraction of component i
z	axial coordinate along the section height, m

Greek symbols

α_{gt}	ratio of external surface area of tubes to gas-solid volume, m^2m^{-3}
$\alpha_{w,ext}$	ratio of external surface area of tubes to gas-solid volume, m^2m^{-3}
$\alpha_{w,int}$	ratio of internal surface area of tubes to gas-solid volume, m^2m^{-3}
ΔH_i	heat of adsorption of component i, J mol^{-1}
ε_c	column void fraction, -
ε_p	particle porosity, -
η_{CO_2}	CO_2 capture (recovery) rate, -
θ	effective delay, s
λ_g	axial heat dispersion coefficient of the gas mixture, W $m^{-1}\ K^{-1}$
λ_{pk}	axial heat dispersion coefficient of the structured packing, W $m^{-1}\ K^{-1}$
μ	gas dynamic viscosity, kg $m^{-1}\ s^{-1}$
ξ	volumetric fraction of the structured packing, -
ρ_f	density of heating/cooling fluid, kg m^{-3}
ρ_g	density of the gas mixture, kg m^{-3}
ρ_p	density of adsorbent particles, kg m^{-3}
ρ_{pk}	density of the structured packing, kg m^{-3}
ρ_w	density of heat exchanger tube wall, kg m^{-3}
τ	time constant of open-loop response, s
τ_c	closed-loop time constant, s
τ_I	controller integral time, s
φ	flue gas feed flow rate divided by nominal value, -

temperature-sensitive adsorption capacity, high regeneration temperature requirement and the negative impact of moisture on their CO_2 capture capacity (Nie et al., 2018).

In the work of Mondino et al., a dynamic, first-principle model was used to evaluate the MBTSA process for post-combustion CO_2 capture from a natural gas combined cycle power plant (Mondino et al., 2019), coal-fired power plant (Mondino et al., 2017) and waste-to-energy plant (Mondino et al., 2022). Simulation results indicate that the MBTSA process can achieve high CO_2 recovery rates and purity of the captured CO_2 for all three applications. In a paper by Morales-Ospino et al., a similar mathematical model was applied in a parametric analysis to investigate how various process variables affected the MBTSA

performance (Morales-Ospino et al., 2021). The specific energy consumption of the process was found to be competitive against commercial amine absorption processes, and up to 99 mol% CO_2 recovery and 91 mol% purity could be achieved. Jung and Lee performed a techno-economic evaluation of CO_2 capture with an amine-functionalized solid sorbent from a coal-fired power plant, reporting that the CO_2 capture cost of a moving bed process was lower than the reference amine-based absorption process (Jung and Lee, 2022). MBTSA has also been demonstrated experimentally at large scale. The KCC process developed by Kawasaki Heavy Industries, which uses an amine-impregnated adsorbent, has been tested at 5 (Okumura et al., 2017) and 40 (Okumura et al., 2018) tons of captured CO_2 per day. This process uses low-grade steam at 60 °C in a direct-contact configuration for regeneration of the adsorbent material. Also, CO_2 capture systems based on fluidized beds with temperature-swing adsorption have been demonstrated at pilot scale. ADA tested an amine functionalized ion-exchange resin sorbent on a 1 MW_e flue gas stream from a coal-fired power plant (Sjostrom and Senior, 2020). KEPCO tested an Na/K carbonate-based capture process on 10 MW_e scale at a coal-fired power plant in Korea, showing that over 80% CO_2 recovery and 95% purity could be achieved (Park et al., 2014).

Most of the studies on MBTSA focus on steady-state operation, but CO_2 capture from thermal power plants will likely need to deviate from steady-state due to expected changes in the energy system. Based on stated policies, the International Energy Agency estimates that renewable energy sources will stand for 43% of global electricity generation in 2030 and 65% in 2050 (IEA, 2022). The intermittent nature of such energy sources represents a challenge since there must always be a balance between supply and demand. Alongside energy storage and demand response measures, the residual load not covered by renewables is expected to be met by flexible operation of fossil-fueled power plants, particularly in the short to medium term (Gonzalez-Salazar et al., 2018). In the case of post-combustion CO_2 capture, variations in the power plant load will require flexible operation of the capture plant. A recent study by Singh et al. concluded that profitable operation of CCS deployed on flexibly operating power plants could be achieved in the future through a combination of market incentives, cost reductions and the use of depreciated assets (Singh et al., 2022). This would further increase the probability of CO_2 capture deployment on thermal power plants. For flexible operation, well-designed process control systems must be developed for the CO_2 capture process to ensure safety and robustness under various uncertainties and disturbances (Hasan et al., 2022). Thus, the main motivation for studying process control in this work is to ensure that the MBTSA process can reliably capture CO_2 from a power plant even under varying operating conditions.

1.2. Process control of post-combustion CO_2 capture

Both decentralized and centralized control structures have been extensively studied in the literature for solvent-based post-combustion CO_2 capture from coal-fired power plants. Most studies consider the CO_2 recovery rate and reboiler temperature as higher-level control variables, using the lean solvent flow rate and reboiler heat duty (or flow rate of extracted steam from the power plant) as manipulated variables (Wu et al., 2020b). In the following paragraphs, a summary of relevant articles within this topic is provided.

Decentralized control structures are based on single input – single output loops, pairing one manipulated variable (MV) with each control variable (CV). They are easy to implement and widely studied in the literature. Lawal et al. (2010) studied a chemical absorption process based on monoethanolamine (MEA) under several dynamic scenarios, using the solvent flow rate to control CO_2 recovery and the reboiler duty to control the reboiler temperature. Based on a relative gain array (RGA) analysis, Gaspar et al. arrived at the same pairing for piperazine and MEA-based processes (Gaspar et al., 2016). Nittaya et al. (2014) studied the reverse pairing (i.e., using the reboiler duty to control CO_2 recovery and solvent flow to control reboiler temperature) and found a heuristic approach to give better performance than RGA analysis. Mechleri et al. used the same MV-CV coupling as Mechleri et al. (2017) to investigate control of a coupled supercritical coal-fired power plant – CO_2 capture process. Using the same control structure as their previous work, Lawal et al. (2012) studied the dynamic behavior of a supercritical power plant integrated with an MEA-based capture process. Gardarsdóttir et al. (2017) compared a range of decentralized control structures using a coupled power plant – CO_2 capture model implemented in Dymola.

In recent years, emphasis has shifted towards centralized control approaches such as model predictive control (MPC). Compared to classical structures, such controllers have the benefit of better handling of coupled control loops and the ability to handle constraints (Akinola et al., 2020). The simplest form of MPC uses linear predictive models in the optimization problem used to determine the control action. An example is the work of Jung et al., which used gap metric analysis to determine the optimal reference point for linear controller design (Jung et al., 2020). The control structure was tested for dynamic simulations of CO_2 recovery setpoint changes and flue gas flow rate variations for a stand-alone capture plant. Rúa et al. used several linear models combined in a local model network for MPC of natural gas combined cycle power plant with solvent-based CO_2 capture (Rúa et al., 2021). A nonlinear artificial neural network predictive model with online updating of weights was studied by Wu et al., combined with particle swarm optimization to solve the optimal control problem (Wu et al., 2020a). The same group studied a supercritical power plant with post-combustion CO_2 capture, using MPC based on state-space models for both sub-processes and considering operation modes prioritizing either the power plant or CO_2 capture (Wu et al., 2019). For similar systems, other recent articles have investigated distributed MPC based on dynamic matrix controllers (Tang and Wu, 2023), linear MPC with state-space models and an extended state observer (Liao et al., 2023) and inverse control using a neural network to predict MV values from CV setpoints instead of the process state (Liao et al., 2020).

As shown above, most studies on control of post-combustion CO_2 capture from thermal power plants have either focused on simple feedback or feedforward controllers or advanced model predictive configurations. Although MPC generally gives improved performance over single-loop control, it is not always recommended. Panahi and Skogestad (2012) and Cormos et al. (2015) both recommended simple control structures over MPC, due to comparable performance and easier implementation.

Enhanced single-loop control is a collective term for advanced control strategies that aim at improving performance beyond what is achievable with single-loop proportional-integral-derivative (PID) controllers without the complexity of MPC (Seborg et al., 2016). Examples of such strategies are time-delay compensation, inferential control, selective and override control, input or output variable transformations, fuzzy logic control and adaptive control. The most commonly applied enhanced single-loop strategy is updating PID controller gains based on operating conditions, a strategy known as gain scheduling (Wei et al., 2014). A few examples from the literature from thermo-mechanical applications are provided here. Modekurti et al. (2017) applied a control structure involving gain scheduling to avoid surge during operation of a multistage CO_2 compression train. Hernandez et al. (2017) demonstrated that a gain-scheduled PID controller showed comparable performance with MPC for a small-scale waste heat recovery system. Cui et al. (2022) adaptively adjusted the controller integral time (keeping the gain constant) for control of superheated steam temperature in a thermal power plant.

Enhanced single-loop control strategies are not widely studied in the literature for post-combustion CO_2 capture but could improve the decentralized control performance of such processes. In this work we focus on two strategies that have been suggested by previous studies but have not yet been evaluated in detail. The strategies are explained in Section 3.1. Firstly, we consider adaptive controller tuning, which

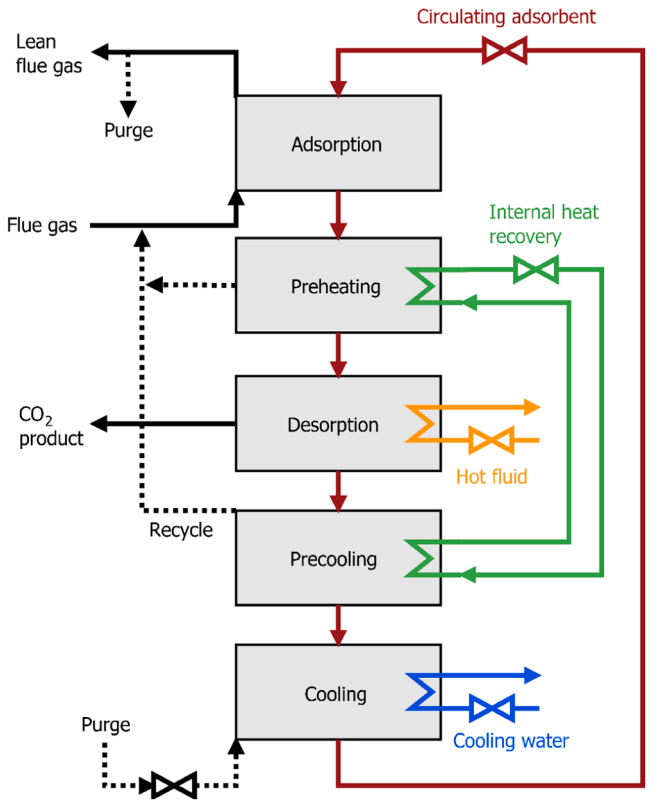

Fig. 1. The moving bed temperature swing adsorption post-combustion CO_2 capture process. The manipulated variables are indicated by valves.

means that a model is used to automatically adjust the tuning parameters based on system conditions. In our previous work (Skjervold et al., 2023), simulations for an activated carbon-based MBTSA process indicated that adaptive tuning could improve the performance and robustness of the controllers. This was especially relevant at lower power plant loads. As shown by the above literature review, adjusting both the controller gain and integral time can be advantageous.

Another recommendation from Skjervold et al. (2023) was that more sophisticated modification of the ratio used in feedforward control of CO_2 recovery is required to avoid steady-state setpoint offsets. Similar suggestions were made by other studies (Gardarsdóttir et al., 2017; Montañés et al., 2017; Posch and Haider, 2013). Based on testing of different control structures at Technology centre Mongstad in Norway, Montañés et al. (2018) suggested that a combined feedforward and feedback structure could lead to fast and stable disturbance rejection. Following these suggestions, the second enhanced single-loop control strategy studied in this work is the application of an outer feedback controller to adjust the ratio used in a feedforward controller for CO_2 recovery. Compared to standalone feedforward control, this combined approach has the advantage of eliminating steady-state setpoint offsets if integral action is included.

In this work, the MBTSA post-combustion capture process is studied as a standalone system, i.e., without a detailed model of the coal-fired power plant. In this approach, variations in power plant operation are treated as external disturbances to the capture plant. The disturbances should therefore be representative of real-life power plant operation. In the CO_2 capture-related studies described above, the control structures are commonly tested for variations in the flue gas flow rate (using ramps or step changes) as well as setpoint changes for higher-level control variables. However, there are other disturbances relevant for power plant operation that could be considered. Variations in flue gas CO_2 concentration can occur due to e.g., changes in boiler operation, leakages in the flue gas ducts and changes in coal composition and quality. A few studies have included such disturbances for solvent-based processes in the form of periodic variations in CO_2 concentration (Cristea et al., 2020), increased CO_2 concentration due to partial oxy-combustion of the coal (Lawal et al., 2010) and a step change in the carbon content of the coal feed (Liao et al., 2023). However, such disturbances have not been considered for an MBTSA-based capture process. Another possible disturbance is variations in the amount and state of extracted steam for regeneration due to changes in power plant operation. Several articles have considered reductions in the steam flow rate due to peaks in electricity demand (Gardarsdóttir et al., 2015; Gaspar et al., 2016; Lawal et al., 2010). To our knowledge, disturbances in the temperature or pressure of the extracted steam have not been considered in the literature.

1.3. Knowledge gaps and scope of paper

From the literature review it is evident that although process control of solvent-based post-combustion CO_2 capture has been widely studied, the MBTSA process has received little attention in this context. This work addresses several knowledge gaps in the literature and the main novel contributions are summarized below:

1) We study a zeolite-based MBTSA process designed for post-combustion CO_2 capture from a large-scale coal-fired power plant. Process control of such a system has not previously been investigated.
2) We investigate two strategies for enhanced single-loop control, namely adaptive controller tuning based on system load and a combined feedback and ratio feedforward controller. Such control strategies have not previously been studied for post-combustion CO_2 capture.
3) We consider disturbances in the flue gas CO_2 concentration and external heat source temperature. These disturbances have not previously been studied for MBTSA-based CO_2 capture.

The research objective of this work is to perform a model-based comparison of the two enhanced single-loop control strategies with a proportional-integral (PI) controller for several types of dynamic scenarios. Controller performance is evaluated both based on graphical comparison and a quantitative metric.

1.4. Article structure

The article is structured as follows. In Section 2 the main principles of the MBTSA process along with the modeling approach and open-loop behavior of key variables are explained. In Section 3 the investigated control structures, applied tuning methods and scenarios for controller testing are described. Results from the dynamic controller testing simulations are presented in Section 4 and discussed in Section 5. The work is concluded in Section 6.

2. Moving bed temperature swing adsorption CO_2 capture process

In this section, the main principles of the MBTSA process are explained, along with a description of the dynamic first-principle model built in gPROMS and the open-loop dynamic behavior of key control variables.

2.1. Process description

The MBTSA process considered in this work is shown in Fig. 1. The process consists of five main stages, through which the moving bed of adsorbent particles passes from top to bottom due to gravity. Flue gas from the power plant is fed at the bottom of the adsorption section, moving in the opposite direction of the moving bed. This counter-

Table 1
System characteristics and nominal boundary conditions for the MBTSA process.

Variable	Value	Unit
Power plant net power output (without CO_2 capture)	642	MW
Total flue gas mass flow rate	804	kg/s
Number of parallel CO_2 capture units	2	–
Hot fluid inlet temperature	2 40	°C
Cooling water inlet temperature	2 0	°C
Flue gas temperature	3 0	°C
Flue gas pressure	1.02	bar
Flue gas mass flow rate per unit	402	kg/s
Flue gas composition:		
CO_2	14.6	mol%
N_2	85.4	mol%

Table 2
Nominal operating conditions and performance of the MBTSA process.

Variable	Value	Unit
Circulating sorbent mass flow rate	1313	kg/s
Sorbent residence time	322.7	s
Lean sorbent CO_2 loading	0.69	mol CO_2/kg
Rich sorbent CO_2 loading	2.12	mol CO_2/kg
Sorbent cyclic CO_2 working capacity	1.43	mol CO_2/kg
CO_2 purity	96.5	mol%
CO_2 recovery	90.0	%
Lean sorbent temperature	3 0	°C
Regenerated sorbent temperature	2 02	°C
External regeneration heat duty	133	MW
Fraction of total heat recovered by inner loop	37.7	%
External cooling duty	110	MW

current configuration gives even distribution of the driving forces for adsorption because CO_2-depleted flue gas at the top of the adsorption section meets CO_2-lean adsorbent material. The adsorption section is operated adiabatically. After leaving the adsorption section, the circulating adsorbent is heated in the preheating section via an internal heat recovery loop and desorption section using an external heat source. Due to a reduction in the CO_2 adsorption capacity at higher temperatures, CO_2 is desorbed from the adsorbent particles and extracted in a high-purity CO_2 stream. An indirect heat transfer configuration is used, meaning the heat source is not directly in contact with the adsorbent material (Knaebel, 2009). Before being transported back to the top of the adsorption section, the circulating adsorbent is brought back to its original temperature by passing through the precooling and cooling section. There are five manipulated variables used for process control: the circulating adsorbent mass flow rate, flow rate of purge gas used in the cooling/precooling section, as well as the flow rate of internal heat recovery fluid, hot fluid and cooling water.

The CO_2 capture process is designed for the flue gas of a supercritical coal-fired power plant with a net power output of 642 MW. The nominal boundary conditions are given in Table 1. Due to the large amount of flue gas, two parallel CO_2 capture units are considered, each handling 50% of the incoming flue gas. It has been assumed that the flue gas consists of a binary mixture of carbon dioxide and nitrogen that has been dried and cooled to 30 °C upstream of the MBTSA unit. Since nitrogen has a stronger affinity towards Zeolite 13X than oxygen and argon (Park et al., 2006), dry flue gas is well approximated by this binary mixture (Merel et al., 2008).

A summary of the nominal operating conditions and performance of the MBTSA process is given in Table 2. At full load, the process delivers CO_2 at a purity of 96.5% with a CO_2 recovery rate of 90.0%. The CO_2 recovery definition used in this work is:

$$\eta_{CO_2} = \frac{\dot{m}_{CO_2,out}}{\dot{m}_{CO_2,in}}. \quad (1)$$

Where $\dot{m}_{CO_2,in}$ is the mass flow of CO_2 in the flue gas feed and $\dot{m}_{CO_2,out}$ is the mass flow of CO_2 in the stream extracted from the desorption section.

2.2. Dynamic process model

The MBTSA process model applied in this work is a modified version of the gPROMS program described in a previous article from our group (Mondino et al., 2019). It was built in gPROMS ModelBuilder version 7.1.1 (PSE, 2023). The model was scaled to match the nominal flue gas mass flow rate of 402 kg/s per unit and necessary model modifications were made to prepare for the implementation and comparison of different control structures. The design parameters were adjusted to give the desired CO_2 product purity and recovery.

For each individual section of the model (i.e., the adsorption, preheating, desorption, precooling and cooling section) a set of partial differential equations are implemented. The model equations and underlying assumptions are identical for each sub-domain, but design parameter values and operating conditions vary between sections. The equations describe the mass, energy and momentum balances and are dynamic and one-dimensional in the spatial domain. Three separate phases are considered, namely the bulk gas phase, solid phase and gas within the macropores of the adsorbent material. The different sections of the model are connected by using the composite modeling capabilities in gPROMS. For completeness, the set of equations, correlations and supplementary information on the model are given in Appendix A.

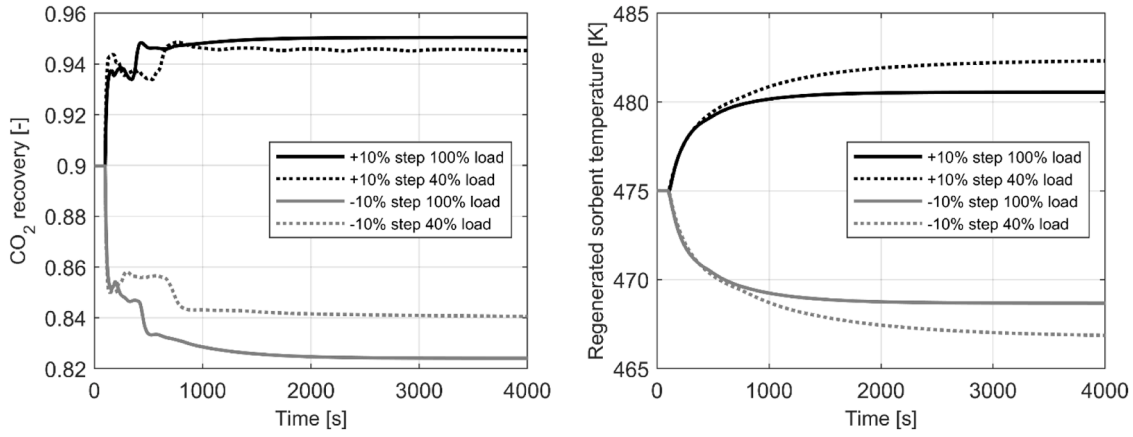

Fig. 2. Open-loop response of CO_2 recovery to step changes in circulating sorbent flow rate (left) and regenerated sorbent temperature to step changes in the flow rate of hot fluid in the desorption section (right). Steps are introduced at $t = 100$ s.

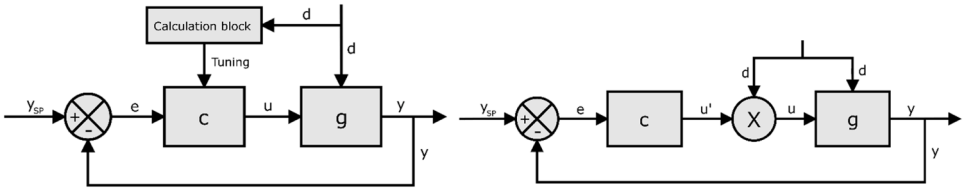

Fig. 3. Enhanced single-loop control strategies investigated in this work. Left: adaptive adjustment of feedback controller tuning based on measured disturbance. Right: combined feedforward and feedback control.

Table 3
Summary of controller tuning parameters and setpoints.

Scheme	CV	MV	τ_c (s)	K_c	τ_I (s)	Setpoint
Std PI	CO_2 recovery	Sorbent mass flow	5.0	99.6	20.0	0.90
	Regenerated sorbent temp	u_f desorption section	16.3	1.65	65.0	475 K
FF + PI	CO_2 recovery (outer loop)	Sorbent / flue gas feed flow ratio	30.6	54.1	115	0.90
	Regenerated sorbent temp	u_f desorption section	16.3	1.65	65.0	475 K
Adaptive Kc	CO_2 recovery	Sorbent mass flow	$\tau/32$	$0.674\varphi + 16.8$	30.6	0.90
	Regenerated sorbent temp	u_f desorption section	$\tau/16$	$0.026\varphi - 0.946$	80.0	475 K
Adaptive $Kc + \tau_I$	CO_2 recovery	Sorbent mass flow	$\tau/32$	$0.674\varphi + 16.8$	$-0.575\varphi + 79$	0.90
	Regenerated sorbent temp	u_f desorption section	$\tau/16$	$0.026\varphi - 0.946$	$-1.36\varphi + 196$	475 K
Regulatory layer	T_s, out cooling section	u_f cooling section	38.1	−0.925	153	303 K
	u_f/sorbent flow ratio in precooling and preheating sections	u_f internal heat recovery loop	–	–	–	0.00019
	u_{out} precooling section	Purge gas mass flow	80.0	1.82	160	0.08 m/s

2.3. Open-loop simulations

Due to a lack of available data in the open literature, it is not possible to validate the complete MBTSA model with experimental results. Therefore, open-loop simulations are necessary to demonstrate that the mathematical model predicts reasonable responses to various changes in operation. Furthermore, the open-loop behavior of the process is the basis for the choice of CV-MV pairings and calculation of controller tuning parameters. Step response simulations were carried out by setting all controllers in manual mode and introducing positive and negative steps of 10% on selected manipulated variables. Simulations at both 100% and 40% power plant load were carried out, to demonstrate the effect of power plant load changes on the open-loop MBTSA process behavior.

In Fig. 2, the responses of CO_2 recovery to sorbent mass flow step changes and regenerated sorbent temperature to desorption section hot fluid flow rate step changes are shown. Previous studies (Morales-Ospino et al., 2021) show that increasing the solid/gas flow rate ratio leads to increased CO_2 recovery and that reduced sorbent flow rates will have a negative effect. Similarly, an increase in the hot fluid flow rate to the desorption section will increase the regenerated sorbent temperature. The figure shows that the model predictions agree with the trends from previous work. The process takes time to settle after a step change has been introduced, since several cycles are required before a new steady-state is reached. The open-loop behavior varies with load, indicating that adaptive adjustment of the controller tuning parameters can be beneficial.

3. Process control

In this section, the process control strategies and controller tuning methods applied in this work are described. The scenarios used to test the investigated control structures are also described.

3.1. Higher-level control structures

As mentioned in Section 1.2, the most common choice of CV-MV pairings for post-combustion CO_2 capture is using the solvent flow rate to control CO_2 recovery and the steam flow rate extracted from the power plant to control the reboiler temperature. In this work, we have followed this pairing strategy for the higher-level control layer. The circulating sorbent mass flow rate is used to control CO_2 recovery and the flow rate of hot fluid in the desorption section is used to control the regenerated sorbent temperature. In the gPROMS model, heat transfer fluid flow rates are represented by their velocity. The regenerated sorbent temperature is closely linked to the CO_2 product purity. As shown in Fig. 2, the input variables have a significant steady-state effect on their respective outputs and short delays, indicating that the chosen pairings are suitable.

Two different types of enhanced single-loop control strategies are investigated in this work, as illustrated in Fig. 3. The first configuration consists of PI controllers with adaptive adjustment of the tuning parameters based on a measured disturbance d (in this case the flue gas feed mass flow rate). The control action is determined by the following equation:

$$u = K_c(\varphi)[P + I(\varphi)](u_{max} - u_{min}) + B. \tag{2}$$

Where u is the calculated value of the manipulated variable, K_c is the controller gain, P is the proportional term, I is the integral term, u_{max} is the upper limit of the manipulated variable, u_{min} is the lower limit of the manipulated variable and B is the controller bias. The flue gas feed mass flow rate normalized by its nominal value, φ, is used in the adaptive tuning relations, as shown in Table 3. The proportional and integral terms are given by:

$$P = e \tag{3}$$

$$\tau_I(\varphi)\frac{dI}{dt} = e \tag{4}$$

Where τ_I is the integral time and e is the controller error. The error is defined as:

$$e = \frac{y_{SP} - y}{y_{max} - y_{min}} \tag{5}$$

Where the subscripts max and min represent the maximum and minimum allowable value of the CV.

In the second configuration, a combination of feedforward and feedback control is used. This configuration is essentially a special type

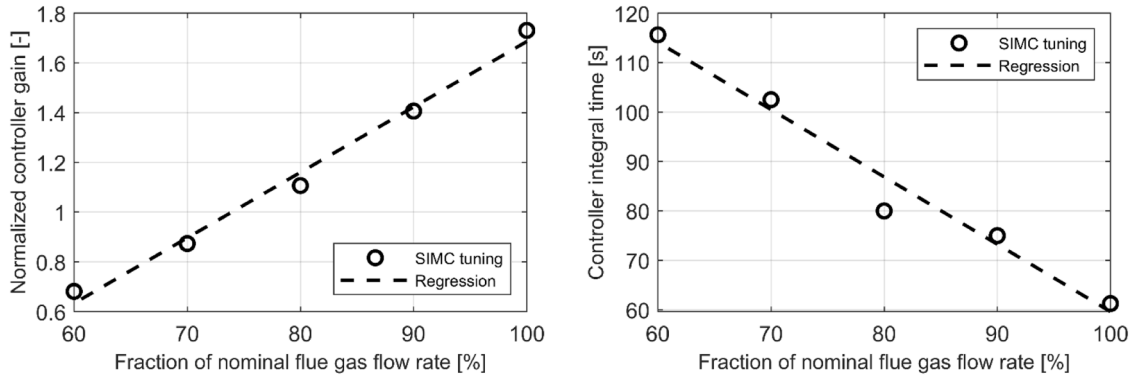

Fig. 4. SIMC tuning parameters for the regenerated sorbent temperature controller vs. fraction of nominal flue gas mass flow rate. The reported values are the average of calculations for positive and negative step responses at each operating point, with $\tau_c = \tau/16$.

of cascade control, where the inner loop is a ratio-type feedforward controller. The control action in such a controller is given by:

$$u = u^{'}d \tag{6}$$

Where the ratio $u^{'}$ is the calculated MV value from the outer feedback loop, given by Eq. (6) with fixed tuning parameters. The integral action included in the outer feedback loop will remove the steady-state setpoint offset typically associated with pure feedforward control.

The enhanced single-loop configurations are compared with a reference case consisting of standard PI controllers with constant tuning. The short name and main characteristics of the control structures studied in this work are summarized below:

1) Std PI: PI controllers with fixed tuning parameters are used to control both the CO_2 recovery and regenerated sorbent temperature (base case).
2) FF + PI: Combined feedforward and feedback control structure for CO_2 recovery, where the ratio used in the feedforward controller is calculated by an outer feedback loop with fixed tuning parameters. The regenerated sorbent temperature controller is identical to the standard PI case.
3) Adaptive K_c: PI control of CO_2 recovery and regenerated sorbent temperature with online adjustment of controller gains based on the system load. The integral times are kept constant.
4) Adaptive $K_c + \tau_I$: PI control of CO_2 recovery and regenerated sorbent temperature with online adjustment of controller gains and integral times based on the system load.

3.2. Regulatory layer

In addition to the higher-level control loops, a regulatory layer is needed to control additional variables needed for stable operation of the process under varying operation. As shown in Fig. 1, three manipulated variables are available for regulatory control after the control loops for CO_2 recovery and regenerated sorbent temperature have been specified. The pairing philosophy and controller configurations for the regulatory layer follow the approach in our previous work (Skjervold et al., 2023), and they are therefore only briefly explained here.

Firstly, the velocity of the working fluid in the internal heat recovery loop is adjusted to maintain a constant ratio with the sorbent mass flow rate. The aim of this controller is to keep the fraction of heat transfer delivered by the internal loop constant throughout varying operation. To maintain the sorbent adsorption capacity during cyclic operation, the particles are cooled to a given temperature before entering the adsorption section. This is achieved by manipulating the velocity of the cooling water flow to the cooling section in a PI controller. Finally, the mass flow rate of purge gas is adjusted in a PI controller with the gas velocity at the top of the precooling section as the controlled variable. The regulatory control structures are identical in all the cases considered in this work.

3.3. Controller tuning

Feedback controller tuning was based on the simplified internal model control (SIMC) rules (Skogestad, 2003). For a PI-controller, a first-order transfer function $g(s)$ describing the open-loop relation between the manipulated and controlled variable is used to calculate the controller tuning parameters:

$$g(s) = \frac{ke^{-\theta s}}{\tau s + 1} \tag{7}$$

Where k is the gain, θ is the effective delay and τ is the time constant of the response. For each CV-MV pairing and considered system load, the parameters of the transfer function were determined from MV step response simulations. The SIMC rules give the controller gain and integral time based on the user-defined closed-loop time constant τ_c:

$$K_c = \frac{1}{k}\frac{\tau}{\tau_c + \theta} \tag{8}$$

$$\tau_I = \min\lfloor \tau, 4(\tau_c + \theta)\rfloor. \tag{9}$$

Since no significant observable delay is seen in the open-loop simulations, the choice of closed-loop time constant is not evident. For each control loop, different values of τ_c were tested before arriving at the controller tuning parameters summarized in Table 3. For the combined feedforward and feedback control structure, a more robust tuning (i.e., larger closed-loop time constant) was chosen, since the gain from MV to CV will vary due to multiplication with the measured disturbance.

In order to determine parametrized tuning relations for the adaptive PI controllers, tuning at several system loads was necessary. For φ-values of 60, 70, 80, 90 and 100%, open-loop simulations with ± 10% MV steps followed by SIMC-based tuning were performed. At each point, the average tuning parameter values from the positive and negative steps were calculated. In Fig. 4, the results for the regenerated sorbent temperature controller are shown as an example. The figure shows that the SIMC controller gain increases and the integral time decreases with increasing φ, indicating that more robust tuning is necessary at lower loads. Linear regression was used to parametrize the variation of K_c and τ_I with φ.

In Table 3, a summary of the tuning parameters and setpoints for the control structures investigated in this work is given.

3.4. Investigated scenarios and quantitative performance metric

A range of scenarios are considered to test the investigated control

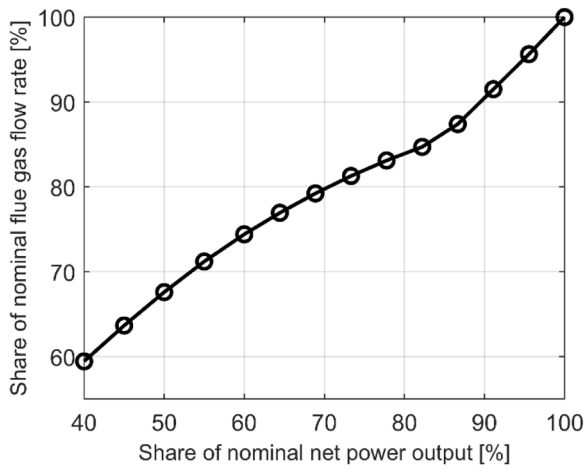

Fig. 5. Relationship between flue gas mass flow rate and nominal net power output, based on part-load simulations (steady-state off-design) in the STEAM MASTER program (Thermoflow Inc, 2023).

structures with cases representative of real-life power plant operation and disturbances. They are listed below:

1) Ramps in power plant load in the 100–40% range.
2) Setpoint changes for CO_2 recovery.
3) Setpoint changes for the regenerated sorbent temperature.
4) Variations in the flue gas feed CO_2 concentration.
5) Variations in the temperature of the external heat source.
6) Delays in the measurement of CO_2 recovery and regenerated sorbent temperature.

No dynamic power plant model has been included, meaning that the scenarios used for controller testing are implemented in the form of variations in the boundary conditions to the MBTSA process. The integral absolute error (IAE) was used to quantify the controller performance. It is defined as:

$$\text{IAE} = \int_0^t |y_{SP}(t) - y(t)|dt \tag{10}$$

Where y_{SP} is the setpoint for a given CV and y is its actual value. A steady-state power plant model in version 30 of the STEAM MASTER program (Thermoflow Inc, 2023) was used to determine the relationship between flue gas mass flow rate and net power output at part-load conditions. The simulation results are shown in Fig. 5 and were used to convert the power plant net power output to a flue gas mass flow rate, which was used as input to the gPROMS model. Ramps in power plant load follow a rate of change of 5% nominal load over a period of 30 s, following the requirement for newly built power units in Poland (Zima et al., 2023).

4. Results from controller test scenarios

In this section, the simulation results are presented and explained. The purpose of these simulations was to test the different control configurations with various dynamic scenarios that could be relevant for a power plant with post-combustion CO_2 capture.

4.1. Power plant load ramps

In Fig. 6, CV and MV responses to ramps in power plant load in the 40–100% load range are shown. To emulate a power plant varying its operation between different loads, ramps from 40 to 60%, 60–80% and 80–100% load were simulated, allowing the controllers to settle over a period of 20 min between each ramp. Only positive ramps were included since ramp-down simulations showed similar relative behavior of the different control configurations. The feedback controllers for adsorbent cooling and precooling gas velocity are included in the results, to show the performance of both control layers over a wide operating range.

Increasing the flue gas feed mass flow rate to the MBTSA process leads to a reduction in CO_2 recovery before the controllers compensate by increasing the circulating sorbent flow rate. The increased sorbent flow causes a reduction in the regenerated sorbent temperature, which is eventually counteracted by an increase in the heating fluid flow to the desorption section. Similarly, the flow of cooling water must be increased to cover the higher cooling duty requirement associated with a larger sorbent flow rate. The main purpose of the purge flow in the cooling and precooling sections is to facilitate transport of gaseous CO_2 from the macropores in the adsorbent to the bulk phase, to avoid re-adsorption of CO_2 as the particles are cooled. When the sorbent flow rate is increased, the gas velocity at the top of the precooling section is reduced due to more CO_2 being re-adsorbed on the particles. This is counteracted by an increase in the purge flow rate. Due to the identical tuning, the regulatory controllers show similar behavior for all configurations.

Since they are more robustly tuned, the adaptive controllers give a slower CO_2 recovery and regenerated sorbent temperature response than the Std PI configuration. As expected, the difference is most evident at lower loads. The MV usage of the adaptive controllers is marginally smoother than the other control schemes. For all CVs, no steady state setpoint offsets are observed in any of the control configurations.

As shown in Table 3, the outer loop in the FF + PI configuration is less aggressively tuned than the other CO_2 recovery controllers. Since the optimal sorbent to flue gas flow ratio varies with load, the FF + PI scheme is dependent on the outer loop to adjust the ratio before the setpoint is reached, leading to a slower CO_2 recovery response. The regenerated sorbent temperature response of the FF + PI configuration is similar to the Std PI case.

4.2. Setpoint changes for CO_2 recovery

In Fig. 7, the response of the higher-level CVs and MVs to CO_2 recovery setpoint changes at 40% power plant load is shown. The recovery setpoint changes from 0.9 to 0.95 and the controllers are allowed to settle before the setpoint is reduced to its original value.

Increasing the CO_2 recovery setpoint requires an increase in the sorbent flow rate, which is followed by an increase in the heating fluid flow to maintain the desired regenerated sorbent temperature. In this case, the adaptively tuned PI controllers show the most efficient CO_2 recovery setpoint tracking, particularly for the positive setpoint change from 0.9 to 0.95. No significant differences between the adaptive K_c and adaptive $K_c + \tau_I$ configurations are observed. The Std PI and FF + PI schemes demonstrate tighter control of the regenerated sorbent temperature.

4.3. Varying flue gas feed CO_2 concentration

In Fig. 8, the closed-loop responses to variations in the flue gas feed CO_2 concentration at 60% load are shown. Firstly, the mol fraction of CO_2 in the flue gas is reduced from 0.146 to 0.135 and the controllers are given time to settle. Subsequently, the CO_2 mol fraction is increased back to its nominal value of 0.146. It is seen from the definition in Eq. (1) that reducing the concentration of CO_2 in the flue gas will give an immediate increase in the CO_2 recovery, which is counteracted by a reduction in the sorbent flow rate. However, a lower CO_2 feed concentration gives less favorable conditions for adsorption, which is expected to lead to a higher sorbent/flue gas ratio than in the nominal case. Ultimately, decreasing the CO_2 feed concentration leads to a reduction in the steady state value of the sorbent mass flow rate.

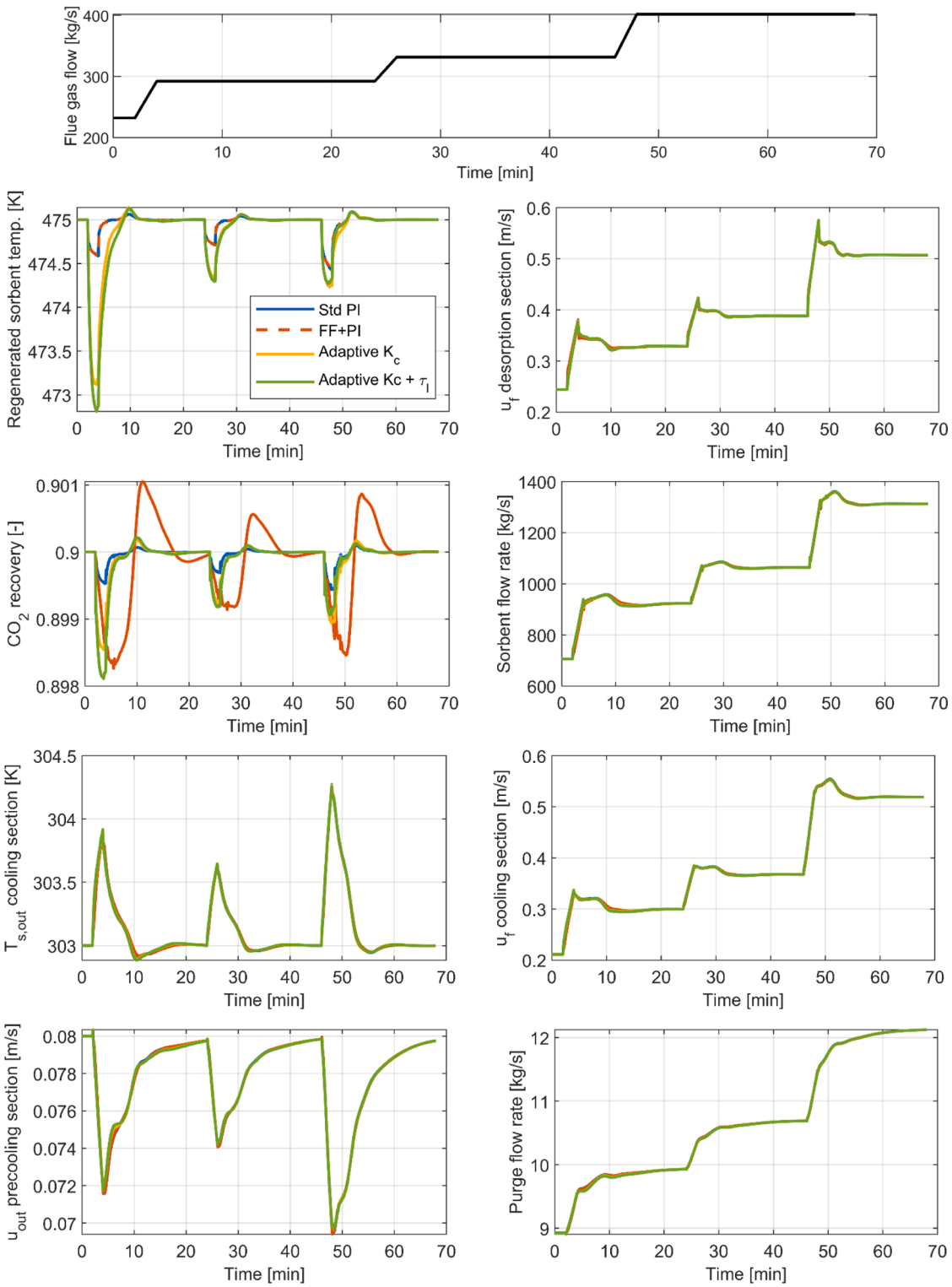

Fig. 6. Response of CVs (left) and MVs (right) to power plant load ramps between 40 and 100%. The top graph shows the variation in flue gas mass flow rate during the simulation.

In this scenario, the FF + PI scheme keeps the CO_2 recovery quite close to the setpoint for both positive and negative CO_2 concentration step changes, but it requires more time to settle due to the more robust tuning. The adaptively tuned controllers and the Std PI configuration show similar disturbance rejection profiles for CO_2 recovery. As in the previous scenarios, the FF + PI and Std PI configurations control the regenerated sorbent temperature most efficiently.

4.4. *Varying external heat source temperature*

In Fig. 9, the responses of higher-level CVs and MVs to a 20 K reduction in the hot fluid inlet temperature at full load are shown. This scenario emulates a change in power plant operation that leads to reduced temperature of the extracted steam to the CO_2 capture process. To maintain similar driving forces for heat transfer as in the nominal

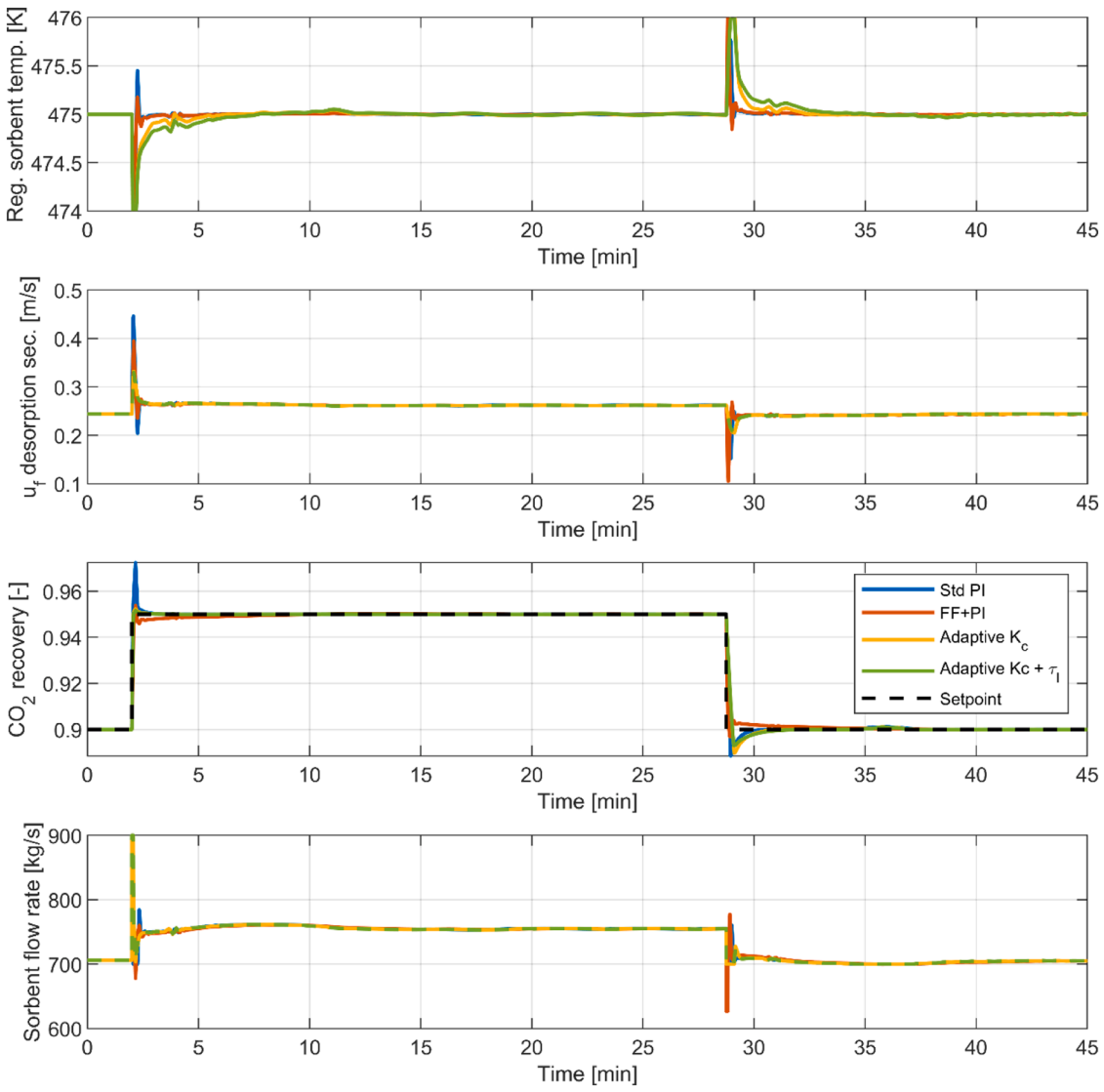

Fig. 7. Response of higher-level CVs and MVs to CO_2 recovery setpoint changes at 40% load.

case, the setpoint for the regenerated sorbent temperature is simultaneously reduced to 455 K. The adaptive cases are not included since they will give almost identical results as the Std PI configuration at full load.

A lower regenerated sorbent temperature increases the lean CO_2 loading of the adsorbent particles entering the adsorption section, leading to a reduction in the cyclic working capacity. To maintain the CO_2 recovery requirement of 90%, a significant increase in the sorbent mass flow rate is observed.

4.5. Effect of measurement delays

When generating the results presented in Sections 4.1–4.4, it was assumed that all measurements and control actions take place without delay. This is not achievable in practice. In this section, the effect of delays on the closed-loop behavior is studied by introducing measurement delays of 15 s for the CO_2 recovery and 5 s for the regenerated sorbent temperature. Compared to the previously presented scenarios, controllers with larger delay margins were required in this case to avoid instabilities. Therefore, the closed-loop time constant was increased to $\tau_c = \tau$ for the Std PI and FF + PI CO_2 recovery controllers and $\tau_c = \tau/4$ for all regenerated sorbent temperature controllers. Since the adaptive controllers are made less aggressive at lower loads, a closed-loop time constant of $\tau_c = \tau/2$ for CO_2 recovery could be applied without causing unstable behavior.

In Fig. 10, the responses of higher-level CVs and MVs to a ramp from 60 to 80% power plant load when considering measurement delays are shown. In the feedforward part of the FF + PI controller, the sorbent flow rate during the ramp is increased independently of the CO_2 recovery measurement. This keeps the CO_2 recovery closer to its setpoint than the other configurations at the start of the simulation. In this scenario, the adaptive control schemes demonstrate tighter control of the CO_2 recovery than the Std PI configuration since they can handle more aggressive tuning. For the regenerated sorbent temperature, a smaller initial reduction is seen for the Std PI case since the sorbent flow rate changes more slowly in this configuration. The shortest regenerated sorbent temperature settling time is observed for the FF + PI controller. In general, the settling times observed in this scenario are longer than in the previous cases, showing that delays have a significant effect on the controllers.

4.6. Summary of quantified controller performance

In Table 4, the IAE values for CO_2 recovery and regenerated sorbent temperature for ramps from 40 to 100% load, recovery setpoint changes

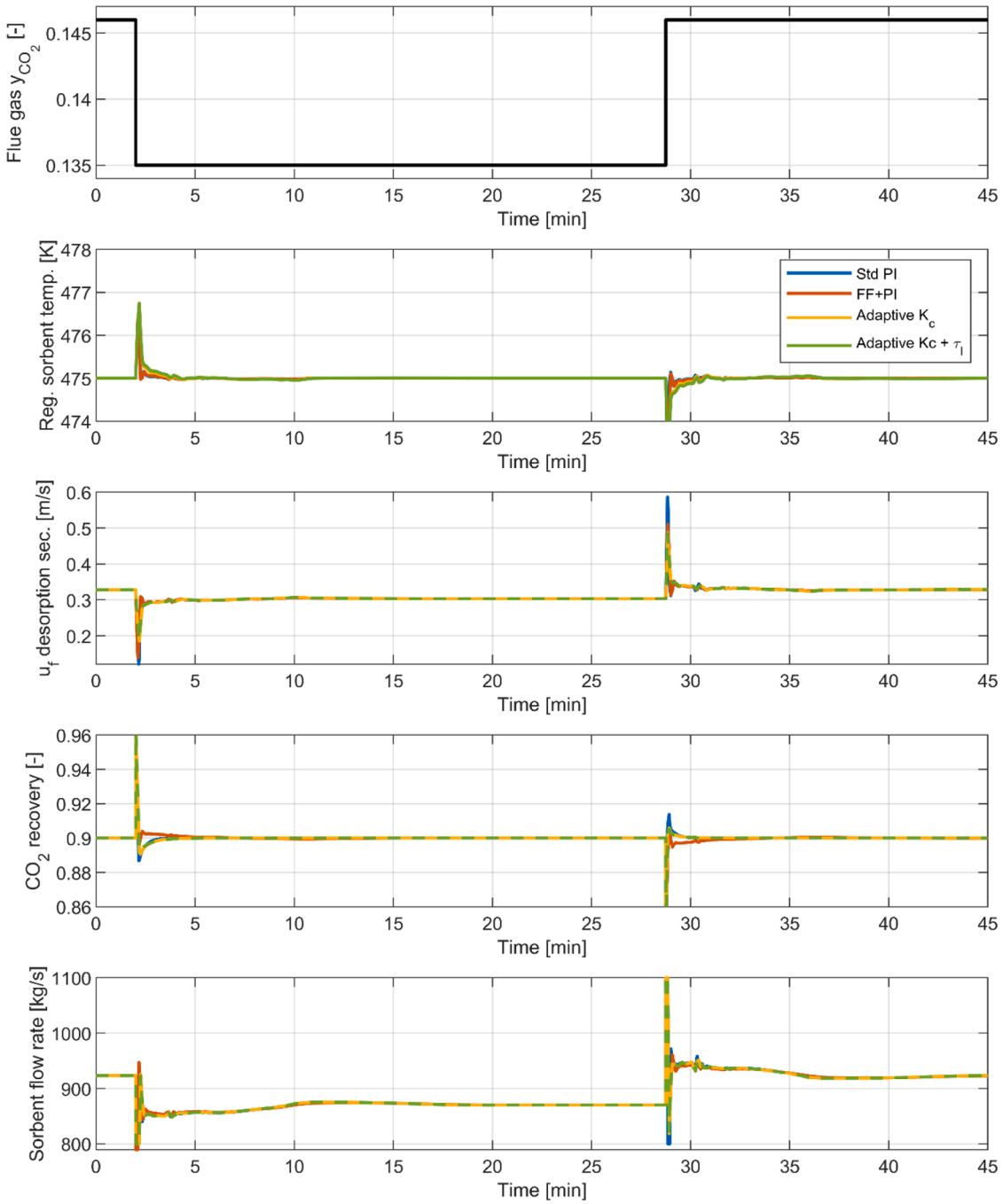

Fig. 8. Response of higher-level CVs and MVs to step changes in flue gas feed CO_2 concentration at 60% load.

at 40% load and flue gas feed CO_2 concentration at 60% load are reported. The selected cases are expected to be representative examples of the relative controller performance without measurement delays.

The Std PI configuration achieved the lowest CO_2 recovery IAE values in all three scenarios. However, similar values are observed for the adaptively tuned PI controllers. Slightly lower IAE values are obtained by adjusting both the integral time and controller gain. For regenerated sorbent temperature, the FF + PI configuration has the lowest IAE values. For this CV, the adaptive $K_c + \tau_I$ configuration has higher IAE values than the adaptive K_c case in all scenarios.

In Table 5, the IAE values for CO_2 recovery and regenerated sorbent temperature for the 60–80% power plant load ramp with measurement delays are given. Since the controllers are slower in this scenario, significantly larger values than in Table 4 are obtained.

5. Discussion

The dynamic scenarios investigated in this work demonstrate the benefits and drawbacks of the enhanced single-loop configurations compared to the standard PI reference case. For the results presented in Sections 4.1–4.4, it was assumed that all variables needed in the control system are measurable without delay and that control actions can be implemented instantaneously. This is not achievable in practice, and these results should therefore be seen as optimistic predictions of controller performance. In these scenarios, the adaptively tuned controllers give smoother and narrower MV profiles than the other configurations, which is important in a real-life installation due to less wear on valves and other process equipment. These controllers also showed the best CO_2 recovery setpoint tracking performance. Modifying both the

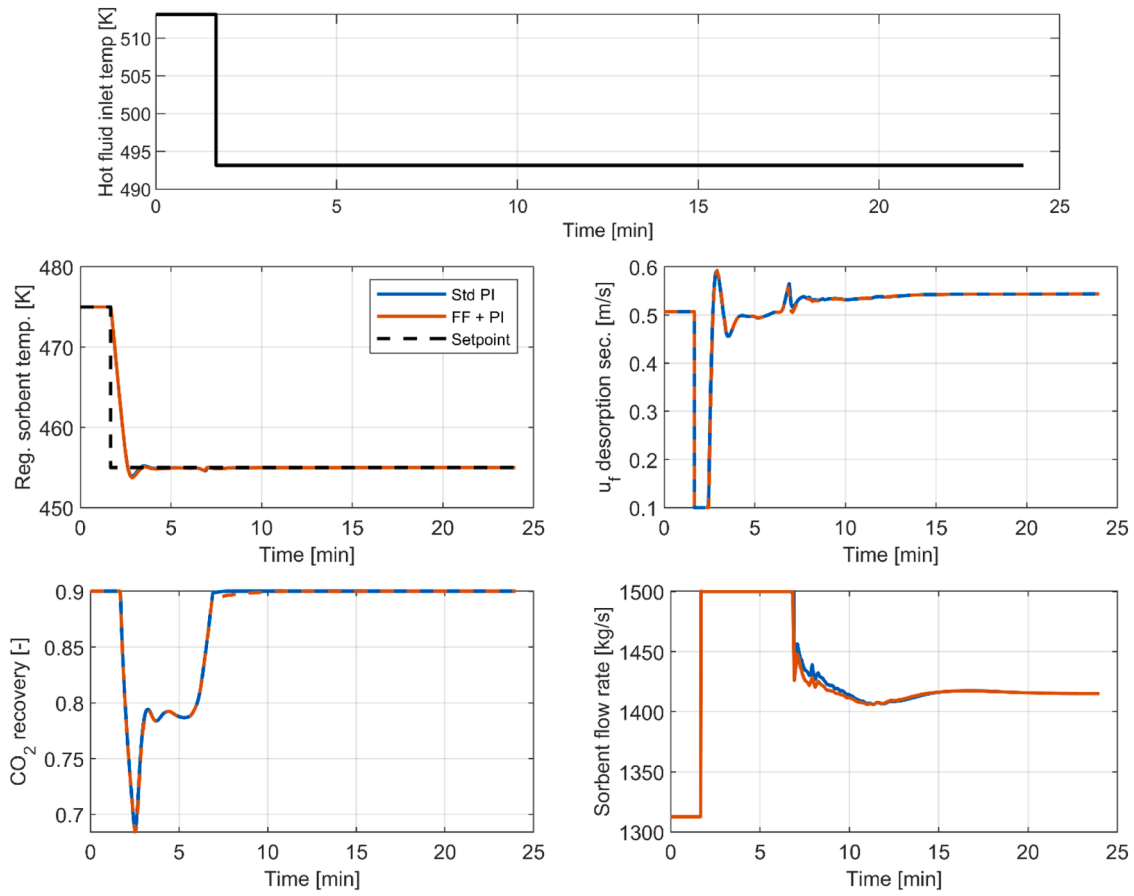

Fig. 9. Response of higher-level CVs and MVs to a simultaneous change in hot fluid inlet temperature and regenerated sorbent temperature setpoint at 100% load. The top graph shows the step change in hot fluid inlet temperature at $t = 1.67$ min.

integral time and controller gain does not significantly improve the controller performance compared to only adjusting the controller gain. This indicates that K_c is the most important parameter for adaptive tuning.

Except for CO_2 feed concentration disturbance rejection, the FF + PI configuration did not improve the control of CO_2 recovery compared to the reference case when no measurement delays were considered. The main benefit of this configuration was better control of the regenerated sorbent temperature. A possible explanation of this improvement is that the combined feedback and feedforward structure contributes to a better decoupling of the recovery and sorbent temperature control loops. This suggests that implementing decoupling approaches such as the one proposed by Shinskey (1977) or the use of model predictive control methods with inherent handling of coupled variables could improve the control of the MBTSA process. More detailed evaluation of this topic and testing of such approaches is left for future work.

In Sections 4.1–4.4, no significant differences between the performance of the different control configurations are observed. Since no delays or noise is considered in these scenarios, the controllers can be tuned with small closed-loop time constants, prioritizing controller speed over robustness. As a result, the settling time is short for all four control schemes and the Std PI configuration would be recommended due to its lower complexity. Another factor contributing to short settling times is the assumption that any change in the sorbent flow rate is instantly introduced in all sections of the MBTSA process.

When measurement delays are considered, the advantages of the enhanced single-loop control schemes compared to the standard PI configuration become more evident. A faster CO_2 recovery response is achieved by the adaptive controllers since they can handle more aggressive controller tuning. The feedforward part of the FF + PI configuration leads to closer CO_2 recovery tracking during changes in power plant load. A more detailed investigation of the effect of delays is suggested for future work. This could include studying delays in the manipulated variable control action, which would be more realistic than the assumption of instantaneous action applied in this work. In practice, measurements can be noisy, for example due to sensor inaccuracies or estimation errors for variables that are not possible to measure directly. To account for this, the effect of signal noise could be considered. This would require even more emphasis on controller robustness. Furthermore, the effect of delays in other types of dynamic scenarios could be studied.

The results from Section 4.4 show that the MBTSA process can maintain the desired CO_2 recovery under disturbances in the external heat source temperature. However, we do not consider the effect of such changes in operation on the specific regeneration duty (SRD) of the process. Since the SRD is an important part of the operating costs of the CO_2 capture plant, it would be interesting to include in future work. The control strategies considered in this work are not able to handle constraints, but using an MPC-based control strategy would allow the consideration of additional variables such as the SRD in the control problem.

6. Conclusion

In the coming years, it is likely that flexible operation of post-combustion CO_2 capture from thermal power plants will be necessary to reduce greenhouse gas emissions in an energy system with increasing shares of variable renewable energy sources. In this context, efficient process control systems for the capture plant are needed to ensure safe and robust operation. This work considers a Zeolite 13X-based moving

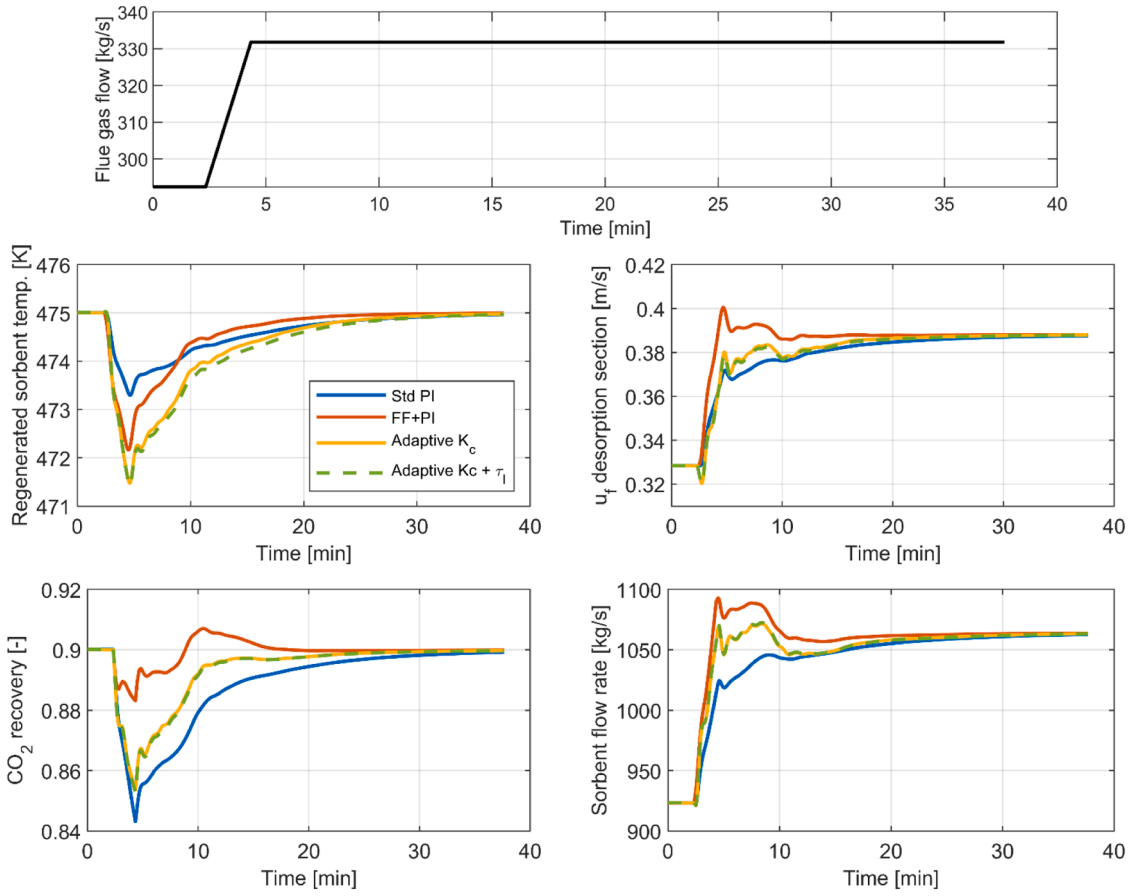

Fig. 10. Response of higher-level CVs and MVs to a ramp from 60 to 80% power plant load with a 15 s delay in the CO_2 recovery measurement and 5 s delay in the regenerated sorbent temperature measurement. The top graph shows the flue gas mass flow rate ramp starting at $t = 1.67$ min.

Table 4
IAE values for CO_2 recovery and regenerated sorbent temperature for selected controller test simulations without measurement delays. The lowest IAE value from each scenario is shown in bold.

	Ramps from 40 to 100% load		Recovery SP changes at 40% load		Flue gas y_{CO_2} steps at 60% load	
Control scheme	IAE CO_2 recovery	IAE reg. sorbent temp.	IAE CO_2 recovery	IAE reg. sorbent temp.	IAE CO_2 recovery	IAE reg. sorbent temp.
Std PI	**0.213**	185.4	**0.925**	37.53	**0.914**	45.64
FF + PI	1.801	**181.0**	1.518	**34.68**	1.477	**42.94**
Adaptive *Kc*	0.534	530.3	0.971	109.2	0.952	83.90
Adaptive *Kc* + τ_I	0.578	593.4	0.946	142.6	0.941	92.14

Table 5
IAE values for CO_2 recovery and regenerated sorbent temperature for a 60–80% power plant load ramp with measurement delays. The lowest IAE value from each scenario is shown in bold.

Control scheme	IAE CO_2 recovery	IAE reg. sorbent temp.
Std PI	25.17	**911.52**
FF + PI	**5.41**	928.13
Adaptive *Kc*	14.63	1491.22
Adaptive *Kc* + τ_I	15.07	1645.80

bed temperature swing adsorption process designed to capture CO_2 from a large-scale coal-fired power plant. The analysis was based on dynamic simulations using a first principle-model built in gPROMS.

Two enhanced single-loop control strategies were implemented and compared with a standard PI configuration. Firstly, adaptive adjustment of the controller gains and integral times based on system load was studied for the CO_2 recovery and the regenerated sorbent temperature. In the second strategy, a cascade approach consisting of a combined feedback and ratio feedforward controller was used to control the CO_2 recovery. In addition to the higher-level control strategies, an identical regulatory control layer was included in all configurations. The different control configurations were tested with several dynamic scenarios that could be relevant for operation of a power plant with post-combustion CO_2 capture. This included power plant load ramps, setpoint changes for CO_2 recovery and regenerated sorbent temperature, variations in flue gas feed CO_2 concentration, changes in the external heat source temperature and the effect of measurement delays. Controller performance was evaluated both based on graphical comparison and using the integral absolute error as a quantitative metric.

All investigated control schemes provided satisfactory performance without steady state offsets, showing that the MBTSA process can be efficiently controlled for different types of scenarios. Nevertheless, the dynamic simulation results revealed benefits and drawbacks of the different approaches. The adaptively tuned controllers gave smoother and narrower manipulated variable profiles than the other configurations and showed the best performance for step changes in the CO_2 recovery setpoint. When measurement delays were included, the adaptive controllers achieved faster CO_2 recovery response for a power plant load

ramp than the reference case. However, these controllers showed less efficient control of the regenerated sorbent temperature. The results indicated that the controller gain is the most important parameter for adaptive tuning. The main benefit of the combined feedback and feed-forward structure in the case of no measurement delays was improved control of the regenerated sorbent temperature. This improvement is possibly caused by better decoupling of the higher-level control loops. When measurement delays were included, this control scheme showed a significant improvement in CO_2 recovery tracking compared to the standard PI configuration.

Several topics can be considered for future work. These include investigation of decoupling approaches for the higher-level control loops and making the mathematical model more representative of real-life operation by including additional delays and signal noise. Furthermore, model predictive control of the MBTSA process could give better handling of coupled variables and allow the inclusion of additional variables such as the specific regeneration duty in the control problem. An MBTSA test stand capturing CO_2 from a coal-fired power plant is currently under construction in Poland as part of the InnCapPlant project (Cracow University of Technology, 2023). Experimental campaigns at this facility will provide valuable information on operation of the process and necessary data for validation of the mathematical model.

CRediT authorship contribution statement

Vidar T. Skjervold: Conceptualization, Formal analysis, Investigation, Methodology, Software, Visualization, Writing – original draft. **Lars O. Nord:** Conceptualization, Funding acquisition, Methodology, Project administration, Supervision, Writing – review & editing.

Declaration of Competing Interest

The authors declare that they have no known competing financial interests or personal relationships that could have appeared to influence the work reported in this paper.

Data availability

Data will be made available on request.

Acknowledgements

We acknowledge financial support from the Polish-Norwegian Research Program for funding the InnCapPlant project (Grant NOR/POLNORCCS/0015/2019-00).

Appendix A Model equations and supplementary information on gPROMS model

The model equations in the gPROMS model are given in Table A.1.

As shown in Table A.1, the Virial model extension for multi-component gas mixtures was applied in this work. It uses the pure component isotherm parameters as input. The Virial model for pure component isotherms is given by:

$$P_i = \frac{q_i^*}{K_i} \mathrm{e}^{\left(A_i q_i^* + B_i q_i^{*2}\right)} \tag{A.1}$$

where P is the pressure, q is the amount of gas adsorbed, and K is the Henry constant. This parameter was calculated with the Van't Hoff equation

$$K_i = K_i^{\infty}\left(\frac{-\Delta H_i}{RT_s}\right) \tag{A.2}$$

and the dependence of the Virial coefficients A and B with temperature was expressed by

$$A_i = A_{0,i} + \frac{A_{1,i}}{T_s} B_i = B_{0,i} + \frac{B_{1,i}}{T_s}. \tag{A.3}$$

Table A1
Model equations.

Mass balance in gas phase	$\varepsilon_c \frac{\partial C_i}{\partial t} + \frac{\partial (uC_i)}{\partial z} = \varepsilon_c \frac{\partial}{\partial z}\left(D_{z,i} C_T \frac{\partial Y_i}{\partial z}\right) - \frac{(1-\varepsilon_c-\xi) a' k_{f,i}}{\mathrm{Bi}_i/5+1}(C_i - C_{p,i})$
Mass balance in macropores	$\varepsilon_p \frac{\partial C_{p,i}}{\partial t} + \nu_s \frac{\partial C_{p,i}}{\partial z} = \varepsilon_p \frac{15 D_{p,i}}{r_p^2} \frac{\mathrm{Bi}_i}{5+\mathrm{Bi}_i}(C_i - C_{p,i}) - \rho_p\left(\frac{\partial q_i}{\partial t} + \nu_s \frac{\partial q_i}{\partial z}\right)$
Mass balance in solid phase	$\frac{\partial q_i}{\partial t} + \nu_s \frac{\partial q_i}{\partial z} = \frac{15 D_{c,i}}{r_c^2}(q_i^* - q_i)$
Momentum bal. (adsorption section)	$-\frac{\partial P}{\partial z} = 2u(1-\varepsilon_c-\xi)(\rho_p - \rho_g)$
Momentum bal. (other sections)	$-\frac{\partial P}{\partial z} = \frac{150\mu(1-\varepsilon_c)^2}{\varepsilon_c^3 d_p^2} u + \frac{1.75(1-\varepsilon_c)\rho_g}{\varepsilon_c^3 d_p}\lvert u\rvert u$
Energy balance in gas phase	$\varepsilon_c C_T \hat{c}_v \frac{\partial T}{\partial t} + uC_T \hat{c}_p \frac{\partial T}{\partial z} = \frac{\partial}{\partial z}\left(\lambda_g \frac{\partial T}{\partial z}\right) - (1-\varepsilon_c-\xi)\, a' h_{gs}(T - T_s) - \alpha_{gt} h_{gw}(T - T_w)$
Energy balance in solid phase	$\left[(1-\varepsilon_c-\xi)\left(\rho_p c_{p,s} + \varepsilon_p \sum_i C_{p,i}\hat{c}_{v,i} + \rho_p \sum_i q_i \hat{c}_{v,i}\right) + \xi \rho_{pk} c_{p,pk}\right]\left(\frac{\partial T_s}{\partial t} + \nu_s \frac{\partial T_s}{\partial z}\right) = (1-\varepsilon_c-\xi)\varepsilon_p R T_s \sum_i \left[\frac{\partial C_{p,i}}{\partial t} + \nu_s \frac{\partial C_{p,i}}{\partial z}\right] + \xi \frac{\partial}{\partial z}\left(\lambda_{pk} \frac{\partial T_s}{\partial z}\right) + (1-\varepsilon_c-\xi) a' h_{gs}(T - T_s) + (1-\varepsilon_c-\xi)\rho_p \sum_i \left(-\Delta H_i\left[\frac{\partial q_i}{\partial t} + \nu_s \frac{\partial q_i}{\partial z}\right]\right)$
Energy balance in the HX-wall	$\rho_w c_{p,w} \frac{\partial T_w}{\partial t} = \alpha_{w,ext} h_{gw}(T - T_w) - \alpha_{w,int} h_{fw}(T_w - T_f)$
Energy balance in the HX-fluid	$\rho_f c_{p,f} \frac{\partial T_f}{\partial t} = -u_f \rho_f c_{p,f} \frac{L_z}{L_x} \frac{\partial T_f}{\partial z} - \alpha_{w,int} h_{fw}(T_f - T_w)$
Adsorption equilibrium	$P_i = \frac{q_i^*}{K_i} \exp\left[\sum_{j=1}^{N} A_{ij} q_j^* + \sum_{j=1}^{N}\sum_{k=1}^{N} B_{ijk} q_j^* q_k^*\right]$ $A_{ij} = \frac{A_i + A_j}{2};\ B_{ijk} = \frac{B_i + B_j + B_k}{3}$

The pure component parameters used in this work are shown in Table A.2.
In Table A.3, the correlations used in the gPROMS model are shown.
In Table A.4, values of fixed parameters used in the model are provided.

Table A2
Pure component virial isotherm parameters for CO_2 and N_2 on Zeolite 13X (Mondino et al., 2019).

	K^{∞} x 10^7 mol/(kg kPa)	− ΔH kJ/mol	A_0 kg/mol	A_1 kg K/mol	B_0 (kg/mol)^2	B_1 kg^{2}K/mol^2
CO_2	1.61935	44.7838	0.4220	7.8371	−0.0485	34.8669
N_2	5.48207	22.6591	−13.037	3889.5	24.961	−7213.8

Table A3
Correlations used in gPROMS model.

Binary diffusivity	$D_{ij} = \frac{0.01883T^{3/2}}{P\sigma_{ij}^2\Omega_{D_{ij}}}\sqrt{\frac{1}{M_{w,i}}+\frac{1}{M_{w,j}}}$
Molecular diffusivity	$D_m = \frac{1-y_i}{\sum_{j\neq i}^{n}\frac{y_j}{D_{ij}}}$
Knudsen diffusivity	$D_k = 97r_p\sqrt{\frac{T}{M_w}}$
Macropore diffusivity	$\frac{1}{D_p} = \tau_p\left(\frac{1}{D_k}+\frac{1}{D_m}\right)$
Axial dispersion coefficient	$D_z = \frac{D_m}{\varepsilon_c}(20 + 0.5\ Sc\ Re)$
Adsorption rate in micropores	$\frac{D_c}{r_c^2} = \frac{D_c^0}{r_c^2}\exp\left(-\frac{E_a}{RT}\right)$
Axial thermal conductivity of gas	$\lambda_g = k_g(7 + 0.5\ \mathrm{Pr}\ Re)$
Sherwood number correlation	$\mathrm{Sh} = 2.0 + 1.1\mathrm{Re}^{0.6}\mathrm{Sc}^{1/3}$
Nusselt number correlation	$\mathrm{Nu} = 2.0 + 1.1\mathrm{Re}^{0.6}\mathrm{Pr}^{1/3}$

Table A4
Values of fixed parameters used in the gPROMS model.

Parameter	Value	Unit	Parameter	Value	Unit
ρ_f	1000	kgm^{-3}	λ_{pk}	0.001	W m^{-1} K^{-1}
ρ_p	924	kgm^{-3}	$c_{p,f}$	4200	J kg^{-1} K^{-1}
ρ_{pk}	1000	kgm^{-3}	$c_{p,pk}$	500	J kg^{-1} K^{-1}
ρ_w	4420	kgm^{-3}	$c_{p,s}$	880	J kg^{-1} K^{-1}
r_p	0.35	mm	$c_{p,w}$	526	J kg^{-1} K^{-1}
ε_c (ads *sec.*)	0.8	–	h_{fw}	5000	W m^{-2} K^{-1}
ε_c (other *sec.*)	0.6	–	h_{gw}	150	W m^{-2} K^{-1}
ε_p	0.34	–	L_x	47.5	m
ξ	0.05	–	L_z	1	m

References

Akinola, T.E., Oko, E., Wu, X., Ma, K., Wang, M., 2020. Nonlinear model predictive control (NMPC) of the solvent-based post-combustion CO_2 capture process. Energy 213, 118840. https://doi.org/10.1016/j.energy.2020.118840.

Cormos, A.M., Vasile, M., Cristea, M.V., 2015. Flexible operation of CO_2 capture processes integrated with power plant using advanced control techniques. Comput. Aided Chem. Eng. 37, 1547–1552. https://doi.org/10.1016/B978-0-444-63577-8.50103-0.

Cracow University of Technology, 2023. InnCapPlant project [WWW Document]. URL https://ke.pk.edu.pl/en/inncapplant-project/ (accessed 5.11.23).

Cristea, V.M., Burca, M.I., Ilea, F.M., Cormos, A.M., 2020. Efficient decentralized control of the post combustion CO_2 capture plant for flexible operation against influent flue gas disturbances. Energy 205, 117960. https://doi.org/10.1016/j.energy.2020.117960.

Cui, X., Xu, P., Song, G., Gu, H., Gu, H., Wang, L., Zhu, H., 2022. PID control of a superheated steam temperature system based on integral gain scheduling. Energies 15, 1–16. https://doi.org/10.3390/en15238978.

Dhoke, C., Zaabout, A., Cloete, S., Amini, S., 2021. Review on reactor configurations for adsorption-based CO_2 capture. Ind. Eng. Chem. Res. 60, 3779–3798. https://doi.org/10.1021/acs.iecr.0c04547.

Dziejarski, B., Krzyżyńska, R., Andersson, K., 2023. Current status of carbon capture, utilization, and storage technologies in the global economy: a survey of technical assessment. Fuel 342. https://doi.org/10.1016/j.fuel.2023.127776.

European Commission, 2019. Communication From The Commission To The European Parliament. The European Council, Brussels. The Council, THE EUROPEAN ECONOMIC AND SOCIAL COMMITTEE AND THE COMMITTEE OF THE REGIONS: The European Green Deal.

Gardarsdóttir, S., Montañés, R.M., Normann, F., Nord, L.O., Johnsson, F., 2017. Effects of CO_2-absorption control strategies on the dynamic performance of a supercritical pulverized-coal-fired power plant. Ind. Eng. Chem. Res. 56, 4415–4430. https://doi.org/10.1021/acs.iecr.6b04928.

Gardarsdóttir, S.Ó., Normann, F., Andersson, K., Prölß, K., Emilsdóttir, S., Johnsson, F., 2015. Post-combustion CO_2 capture applied to a state-of-the-art coal-fired power plant-The influence of dynamic process conditions. Int. J. Greenh. Gas Control 33, 51–62. https://doi.org/10.1016/j.ijggc.2014.12.001.

Gaspar, J., Ricardez-Sandoval, L., Jørgensen, J.B., Fosbøl, P.L., 2016. Controllability and flexibility analysis of CO_2 post-combustion capture using piperazine and MEA. Int. J. Greenh. Gas Control 51, 276–289. https://doi.org/10.1016/j.ijggc.2016.06.003.

Gonzalez-Salazar, M.A., Kirsten, T., Prchlik, L., 2018. Review of the operational flexibility and emissions of gas- and coal-fired power plants in a future with growing renewables. Renew. Sustain. Energy Rev. 82, 1497–1513. https://doi.org/10.1016/j.rser.2017.05.278.

Hasan, M.M.F., Zantye, M.S., Kazi, M.K., 2022. Challenges and opportunities in carbon capture, utilization and storage: a process systems engineering perspective. Comput. Chem. Eng. 166, 107925 https://doi.org/10.1016/j.compchemeng.2022.107925.

Hernandez, A., Desideri, A., Gusev, S., Ionescu, C.M., Van Den Broek, M., Quoilin, S., Lemort, V., De Keyser, R., 2017. Design and experimental validation of an adaptive control law to maximize the power generation of a small-scale waste heat recovery system. Appl. Energy 203, 549–559. https://doi.org/10.1016/j.apenergy.2017.06.069.

IEA, 2023. CO2 Emissions in 2022. Paris.

IEA, 2022. World Energy Outlook 2022. Paris.

IEA, 2020. The role of CCUS in low-carbon power systems. Paris.

IPCC, 2018. Global Warming of 1.5°C. An IPCC Special Report on the impacts of global warming of 1.5°C above pre-industrial levels and related global greenhouse gas emission pathways, in the context of strengthening the global response to the threat of climate change.

Jung, H., Im, D., Heo, S., Kim, B., Lee, J.H., 2020. Dynamic analysis and linear model predictive control for operational flexibility of post-combustion CO_2 capture processes. Comput. Chem. Eng. 140 https://doi.org/10.1016/j.compchemeng.2020.106968.

Jung, W., Lee, J., 2022. Economic evaluation for four different solid sorbent processes with heat integration for energy-efficient CO_2 capture based on PEI-silica sorbent. Energy 238, 121864. https://doi.org/10.1016/j.energy.2021.121864.

Kazemifar, F., 2022. A review of technologies for carbon capture, sequestration, and utilization: cost, capacity, and technology readiness. Greenh. Gases Sci. Technol. 12, 200–230. https://doi.org/10.1002/ghg.2131.

Knaebel, K.S., 2009. Temperature swing adsorption system. US8353978B2.

Lawal, A., Wang, M., Stephenson, P., Koumpouras, G., Yeung, H., 2010. Dynamic modelling and analysis of post-combustion CO_2 chemical absorption process for coal-fired power plants. Fuel 89, 2791–2801. https://doi.org/10.1016/j.fuel.2010.05.030.

Lawal, A., Wang, M., Stephenson, P., Obi, O., 2012. Demonstrating full-scale post-combustion CO_2 capture for coal-fired power plants through dynamic modelling and simulation. Fuel 101, 115–128. https://doi.org/10.1016/j.fuel.2010.10.056.

Liao, P., Li, Y., Wu, X., Wang, M., Oko, E., 2020. Flexible operation of large-scale coal-fired power plant integrated with solvent-based post-combustion CO_2 capture based on neural network inverse control. Int. J. Greenh. Gas Control 95, 102985. https://doi.org/10.1016/j.ijggc.2020.102985.

Liao, P., Wu, X., Wang, M., Li, Z., Qian, F., 2023. Robust control and flexible operation for commercial-scale coal-fired power plant with solvent-based post-combustion carbon capture. Int. J. Greenh. Gas Control 123, 103831. https://doi.org/10.1016/j.ijggc.2023.103831.

Montañés, R.M., GarÐarsdóttir, S.O., Normann, F., Johnsson, F., Nord, L.O., 2017. Demonstrating load-change transient performance of a commercial-scale natural gas combined cycle power plant with post-combustion CO_2 capture. Int. J. Greenh. Gas Control 63, 158–174. https://doi.org/10.1016/j.ijggc.2017.05.011.

Mechleri, E., Lawal, A., Ramos, A., Davison, J., Mac Dowell, N., 2017. Process control strategies for flexible operation of post-combustion CO_2 capture plants. Int. J. Greenh. Gas Control 57, 14–25. https://doi.org/10.1016/j.ijggc.2016.12.017.

Merel, J., Clausse, M., Meunier, F., 2008. Experimental investigation on CO_2 post-combustion capture by indirect thermal swing adsorption using 13X and 5A zeolites. Ind. Eng. Chem. Res. 47, 209–215. https://doi.org/10.1021/ie071012x.

Modekurti, S., Eslick, J., Omell, B., Bhattacharyya, D., Miller, D.C., Zitney, S.E., 2017. Design, dynamic modeling, and control of a multistage CO_2 compression system. Int. J. Greenh. Gas Control 62, 31–45. https://doi.org/10.1016/j.ijggc.2017.03.009.

Mondino, G., Grande, C.A., Blom, R., 2017. Effect of gas recycling on the performance of a moving bed temperature-swing (MBTSA) process for CO_2 capture in a coal fired power plant context. Energies 10. https://doi.org/10.3390/en10060745.

Mondino, G., Grande, C.A., Blom, R., Nord, L.O., 2022. Evaluation of MBTSA technology for CO_2 capture from waste-to-energy plants. Int. J. Greenh. Gas Control 118, 103685. https://doi.org/10.1016/j.ijggc.2022.103685.

Mondino, G., Grande, C.A., Blom, R., Nord, L.O., 2019. Moving bed temperature swing adsorption for CO_2 capture from a natural gas combined cycle power plant. Int. J. Greenh. Gas Control 85, 58–70. https://doi.org/10.1016/j.ijggc.2019.03.021.

Montañés, R.M., Fløø, N.E., Nord, L.O., 2018. Experimental results of transient testing at the amine plant at Technology Centre Mongstad: open-loop responses and performance of decentralized control structures for load changes. Int. J. Greenh. Gas Control 73, 42–59. https://doi.org/10.1016/j.ijggc.2018.04.001.

Morales-Ospino, R., Santos, V.N., Lima, A.R.A., Torres, A.E.B., Vilarrasa-García, E., Bastos-Neto, M., Cavalcante, C.L., Azevedo, D.C.S., Marques, C.R.M., De Aquino, T. F., Vasconcelos, L.B., Knaebel, K.S., 2021. Parametric analysis of a moving bed temperature swing adsorption (MBTSA) process for postcombustion CO_2 capture. Ind. Eng. Chem. Res. https://doi.org/10.1021/acs.iecr.0c05067.

Nie, L., Mu, Y., Jin, J., Chen, J., Mi, J., 2018. Recent developments and consideration issues in solid adsorbents for CO_2 capture from flue gas. Chin. J. Chem. Eng. 26, 2303–2317. https://doi.org/10.1016/j.cjche.2018.07.012.

Nittaya, T., Douglas, P.L., Croiset, E., Ricardez-Sandoval, L.A., 2014. Dynamic modelling and control of MEA absorption processes for CO_2 capture from power plants. Fuel 116, 672–691. https://doi.org/10.1016/j.fuel.2013.08.031.

Okumura, T., Yoshizawa, K., Nishibe, S., Iwasaki, H., Kazari, M., Hori, T., 2017. Parametric testing of a pilot-scale design for a moving-bed CO_2 capture system using low-temperature steam. Energy Procedia 114, 2322–2329. https://doi.org/10.1016/j.egypro.2017.03.1369.

Okumura, T., Yoshizawa, K., Numaguchi, R., Nishibe, S., Kanou, A., Hasegawa, Y., Inoue, S., Tsuji, K., Fujita, S., Nabeshima, M., Yamada, H., Yamamoto, S., Takayama, N., Yogo, K., 2018. Demonstration plant of the kawasaki CO_2 capture (KCC) system with solid sorbent for coal-fired power station. SSRN Electron. J. https://doi.org/10.2139/ssrn.3365953.

Panahi, M., Skogestad, S., 2012. Economically efficient operation of CO_2 capturing process. Part II. Design of control layer. Chem. Eng. Process. Process Intensif. 52, 112–124. https://doi.org/10.1016/j.cep.2011.11.004.

Park, Y.C., Jo, S.H., Kyung, D.H., Kim, J.Y., Yi, C.K., Ryu, C.K., Shin, M.S., 2014. Test operation results of the 10 MWe-scale dry-sorbent CO_2 capture process integrated with a real coal-fired power plant in Korea. Energy Procedia 63, 2261–2265. https://doi.org/10.1016/j.egypro.2014.11.245.

Park, Y.J., Lee, S.J., Moon, J.H., Choi, D.K., Lee, C.H., 2006. Adsorption equilibria of O_2, N_2, and Ar on carbon molecular sieve and zeolites 10X, 13X, and LiX. J. Chem. Eng. Data 51, 1001–1008. https://doi.org/10.1086/505023.

Posch, S., Haider, M., 2013. Dynamic modeling of CO2 absorption from coal-fired power plants into an aqueous monoethanolamine solution. Chem. Eng. Res. Des. 91, 977–987. https://doi.org/10.1016/j.cherd.2012.09.016.

PSE, 2023. gPROMS ModelBuilder [WWW Document]. URL https://www.psenterprise.com/products/gproms/modelbuilder (accessed 3.29.23).

Raganati, F., Miccio, F., Ammendola, P., 2021. Adsorption of carbon dioxide for post-combustion capture: a review. Energy Fuels 35, 12845–12868. https://doi.org/10.1021/acs.energyfuels.1c01618.

Rúa, J., Hillestad, M., Nord, L.O., 2021. Model predictive control for combined cycles integrated with CO_2 capture plants. Comput. Chem. Eng. 146 https://doi.org/10.1016/j.compchemeng.2020.107217.

Samanta, A., Zhao, A., Shimizu, G.K.H., Sarkar, P., Gupta, R., 2012. Post-combustion CO_2 capture using solid sorbents: a review. Ind. Eng. Chem. Res. 51, 1438–1463. https://doi.org/10.1021/ie200686q.

Seborg, D., Edgard, T., Mellichamp, D., Doyle, F., 2016. Process Dynamics and Control, 4th ed. John Wiley & Sons, Hoboken, NJ.

Shinskey, F.G., 1977. The stability of interacting control loops with and without decoupling. IFAC Proc. 10, 21–30. https://doi.org/10.1016/B978-0-08-022010-9.50008-6. Vol.

Singh, S.P., Ku, A.Y., Macdowell, N., Cao, C., 2022. Profitability and the use of flexible CO_2 capture and storage (CCS) in the transition to decarbonized electricity systems. Int. J. Greenh. Gas Control 120. https://doi.org/10.1016/j.ijggc.2022.103767.

Sjostrom, S., Senior, C., 2020. Pilot testing of CO_2 capture from a coal-fired power plant - Part 2: results from 1-MWe pilot tests. Clean Energy 4, 12–25. https://doi.org/10.1093/ce/zkz034.

Skjervold, V.T., Mondino, G., Riboldi, L., Nord, L.O., 2023. Investigation of control strategies for adsorption-based CO_2 capture from a thermal power plant under variable load operation. Energy 268, 126728. https://doi.org/10.1016/j.energy.2023.126728.

Skogestad, S., 2003. Simple analytic rules for model reduction and PID controller tuning. J. Process Control 13, 291–309. https://doi.org/10.4173/mic.2004.2.2.

Tang, Z., Wu, X., 2023. Distributed predictive control guided by intelligent reboiler steam feedforward for the coordinated operation of power plant-carbon capture system. Energy 267, 126568. https://doi.org/10.1016/j.energy.2022.126568.

Thermoflow Inc, 2023. STEAM PRO and STEAM MASTER [WWW Document]. URL https://www.thermoflow.com/products_conventionalsteam.html (accessed 3.30.23).

Wei, G., Wang, Z., Li, W., Ma, L., 2014. A survey on gain-scheduled control and filtering for parameter-varying systems. Discret. Dyn. Nat. Soc. https://doi.org/10.1155/2014/105815.

Wu, X., Shen, J., Wang, M., Lee, K.Y., 2020a. Intelligent predictive control of large-scale solvent-based CO_2 capture plant using artificial neural network and particle swarm optimization. Energy 196, 117070. https://doi.org/10.1016/j.energy.2020.117070.

Wu, X., Wang, M., Liao, P., Shen, J., Li, Y., 2020b. Solvent-based post-combustion CO_2 capture for power plants: a critical review and perspective on dynamic modelling, system identification, process control and flexible operation. Appl. Energy 257, 113941. https://doi.org/10.1016/j.apenergy.2019.113941.

Wu, X., Wang, M., Shen, J., Li, Y., Lawal, A., Lee, K.Y., 2019. Flexible operation of coal fired power plant integrated with post combustion CO_2 capture using model predictive control. Int. J. Greenh. Gas Control 82, 138–151. https://doi.org/10.1016/j.ijggc.2018.12.004.

Zhao, R., Liu, L., Zhao, L., Deng, S., Li, S., Zhang, Y., 2019. A comprehensive performance evaluation of temperature swing adsorption for post-combustion carbon dioxide capture. Renew. Sustain. Energy Rev. 114, 109285 https://doi.org/10.1016/j.rser.2019.109285.

Zima, W., Grądziel, S., Cebula, A., Rerak, M., Kozak-Jagieła, E., Pilarczyk, M., 2023. Mathematical model of a power boiler operation under rapid thermal load changes. Energy 263. https://doi.org/10.1016/j.energy.2022.125836.